Growing length scale in gravity-driven dense granular flow

Shubha Tewari* and Bidita Tithi
Department of Physics, Mount Holyoke College, 50 College Street, South Hadley, Massachusetts 01075, USA

Allison Ferguson
Department of Biochemistry, University of Toronto, Toronto, Ontario M5S 1A8, Canada

Bulbul Chakraborty†
Martin Fisher School of Physics, Brandeis University, Mailstop 057, Waltham, Massachusetts 02454-9110, USA
(Received 14 June 2008; revised manuscript received 24 October 2008; published 27 January 2009)

We report simulations of a two-dimensional, dense, bidisperse system of inelastic hard disks falling down a vertical tube under the influence of gravity. We examine the approach to jamming as the average flow of particles down the tube is slowed by making the outlet narrower. Defining coarse-grained velocity and stress fields, we study two-point temporal and spatial correlation functions of these fields in a region of the tube where the time-averaged velocity is spatially uniform. We find that fluctuations in both velocity and stress become increasingly correlated as the system approaches jamming. We extract a growing length scale and time scale from these correlations.

DOI: 10.1103/PhysRevE.79.011303 PACS number(s): 45.70.−n, 81.05.Rm, 83.10.Pp

I. INTRODUCTION

Granular materials (powders, seeds, grains, sand) consist of macroscopic particles that interact via dissipative short-ranged or contact forces [1]. Granular systems are athermal, since the characteristic energies needed to move a single grain are many orders of magnitude larger than thermal energies. In the absence of external forces, there is no motion, and the state of the system under the application of external forces varies with the magnitude of the force as well as with the packing density of the grains. In this paper, we will describe results from numerical simulations of the dense gravity-driven flow of grains down a vertical tube, as in an hourglass, and the transition from a flowing state to one that is stuck, or jammed.

The questions addressed here fall within the rubric of a proposal [2] to unify disparate systems under a common framework, which posits that there are some universal aspects to the slowing down of the dynamics in many disordered systems as they move from a mobile state to one that is frozen; such a transition is labeled a jamming transition. There is no static structural signature of the transition from a mobile to a jammed state: unlike first-order freezing transitions, there is no discontinuous change in the density or broken translational symmetry. Nor is there a clear signature of a diverging length scale derived from a two-point static correlation function as in a second-order phase transition, though there are other indications of a diverging length scale as a critical density is approached [3–5].

A dense column of grains in a vertical hopper flows down at a steady rate rather than accelerating under gravity because the weight of the column is supported by the walls. The rate of flow decreases as the size of the opening at the outlet of the hopper is decreased and ultimately jams when the opening is a few particle diameters across. It is well known that the distribution of load in a static column of sand is spatially inhomogeneous and organized along linear structures called force chains [6,7]. The question remains open as to whether these structures begin to form in the flowing state as the flow slows. In this article, we present evidence from simulations for increasing spatial correlations in both velocity and stress fluctuations as the flow rate decreases. We extract a length scale from these correlations and find that the flow rate dependence of the length scales for velocity and stress are in exact correspondence. Recent experiments have characterized in detail fluctuations in velocity [8,9] and stress [10] in granular flows. Our results agree very well with experimental observations [11] of growing spatial correlations in velocity fluctuations as the flow in a vertical hopper approaches the jamming threshold and help clarify how these correlations arise in a flow that is dense, continuous, and highly collisional.

There have been many efforts towards extracting a length scale in granular systems. Inhomogeneous force chains were visualized in sheared systems using photoelastic beads [12] and their spatial correlations quantified [13]—these observations have been primarily in the quasistatic regime, where the beads stay in contact rather than undergoing collisions. Force measurements using a photoelastic plate at the base of a sheared, cylindrical pack of beads found a change in the distribution of forces as jamming was approached [14]. Earlier measurements in flow in a rotating drum [15] found evidence of clustering, but with a power-law distribution of cluster sizes and hence no chosen length scale. Growing spatial correlations were seen at the free surface of chute flow down a plane [16], with a length scale of the order of a few grain diameters. Previous simulations of flow in a vertical tube geometry indicated an inhomogeneous distribution of stresses [17]. Earlier results [18] on the same simulations we report on in this article indicated that the most frequently colliding particles organize into chainlike structures that

*stewari@mtholyoke.edu
†bulbul@brandeis.edu

form repeatedly and break up as the particles move down the hopper. It was found that the chain direction coincided with the principal axis of the collisional stress in the system, with the lifetime of correlations in the stress fluctuations increasing with decreasing flow rate [19]. There was quantitative agreement between the simulational results and experiments in a two-dimensional hopper geometry [10,11].

The absence of a clear structural signature of the approach to jamming has led various groups to look for spatial inhomogeneities in the dynamics. This approach was pioneered in structural glasses where a variety of techniques probing local response functions showed [20] that the dynamics of a sample became increasingly heterogeneous near the glass transition. Two-point correlation functions did not show clear signatures of heterogeneity; however, an analysis of four-point correlation functions in simulations of supercooled liquids [21,22] showed evidence for growing spatial correlations between localized density autocorrelations. Evidence for dynamic heterogeneity was found in experiments in colloidal glasses, in which highly mobile particles were found to cluster [23], with a cluster size that increased as the glass transition was approached. Heterogeneous dynamics has now also been seen in experiments on dense granular material under shear [24]. In our simulations as well, spatial heterogeneities were found in the mean-squared displacements of particles when a method [25] of maximizing the difference between highly mobile and less mobile regions of the sample was used [26]. While the size of the spatial heterogeneity varied between five and six particle diameters as a function of flow velocity, the "cage size" or length scale over which the heterogeneity was maximized did increase as the flow velocity decreased towards jamming. However, this increase in length scale was typically smaller than a particle diameter, and the connection with the collisional dynamics and force chains was not clear.

In the current paper, we analyze the development of spatial correlations in both kinetic and dynamical variables in the flowing state, and show that the extent of these increases as jamming is approached. We would like to emphasize that the changing length scale is seen in the two-point correlation functions of the velocity and stress. We also draw qualitative connections between these correlations and the chains of frequently colliding particles.

In the sections to follow, we first describe the simulation and our method of defining coarse-grained velocity and stress fields. We then discuss our results for the time-averaged fields and the temporal and spatial correlations in both velocity and stress fluctuations and conclude with a discussion of our results.

II. DESCRIPTION OF SIMULATION

The results we describe here are obtained from a two-dimensional event-driven simulation of bidisperse hard disks falling under the influence of gravity in a vertical hopper. We use the same particle dynamics as Denniston and Li [17] and have described our setup in some detail in an earlier paper [19]. To summarize, the interparticle collisions are instantaneous and inelastic, and there is no friction between the particles. As a result, momentum transfer between colliding particles always occurs along the vector separating their centers. The relative velocity between colliding particles i and j is reduced by a coefficient of restitution μ, defined in the usual way:

$$(\boldsymbol{u}_j' - \boldsymbol{u}_i') \cdot \hat{\boldsymbol{q}} = -\mu(\boldsymbol{u}_j - \boldsymbol{u}_i) \cdot \hat{\boldsymbol{q}}, \tag{1}$$

where $\boldsymbol{u}_j'$ and $\boldsymbol{u}_i'$ are the particle velocities after the collision, and $\hat{q}$ is a unit vector along the line separating the centers of the particles. Frictional effects at the wall are simulated by introducing a coefficient of restitution, μ_{wall}, for the velocity component parallel to the walls: the loss of vertical momentum at the walls is what allows the flow to reach a steady state. In order to avoid inelastic collapse, all collisions become elastic when the relative velocity at the collision is below a certain threshold u_{cut}. A particle exiting the base has a probability p of being reflected; otherwise, it exits the system and is reintroduced at the top. The flow rate of particles in steady state is controlled by the size of the opening at the base. The results described here are for a simulation of 1000 particles of diameter 1 and 1.2, respectively, where grains are chosen at random to have one or the other size. The other simulation parameters are $\mu=0.8$, $\mu_{\text{wall}}=0.5$, $p=0.5$, and $u_{\text{cut}}=10^{-3}$, and the mass of the smaller grains is set to 1. Lengths are expressed in units of the smaller particle diameter. In these units, the rectangular region of the hopper has width 20 and height 76.5. The simulation is run for a total of 1000 simulation time steps, of which the first 500 are discarded. In units of the simulation time, the average time between collisions for a given particle is on the order of 10^{-3}.

Earlier results reported on these simulations [18,19] were based on a particle-based analysis of the system as the size of the opening, or the flow rate, was decreased. Over a time scale larger than a typical collision time, but shorter than the time taken for a particle to fall through its own diameter, particles with the highest frequency of collisions appear to repeatedly organize into linear structures that form and break. These structures were shown to carry much of the collisional stress [19], and their lifetime increased with decreasing flow rate, but no evidence was found for a growing length scale.

In this paper, we seek to go beyond the particle-level analysis of the system in order to quantify the correlations signaled by the frequently colliding chains of particles and look for indications of increasing order in the system as it approaches jamming. Thus, in the work described here, we have constructed coarse-grained variables, looking at the system in terms of velocity, stress and density fields, and the spatial and temporal variations of these fields. We also view this approach as a useful first step in developing a continuum description of granular flow.

III. RESULTS

A. Coarse-grained fields

The system area is divided into square boxes of side equal to two particle diameters. We define a box velocity

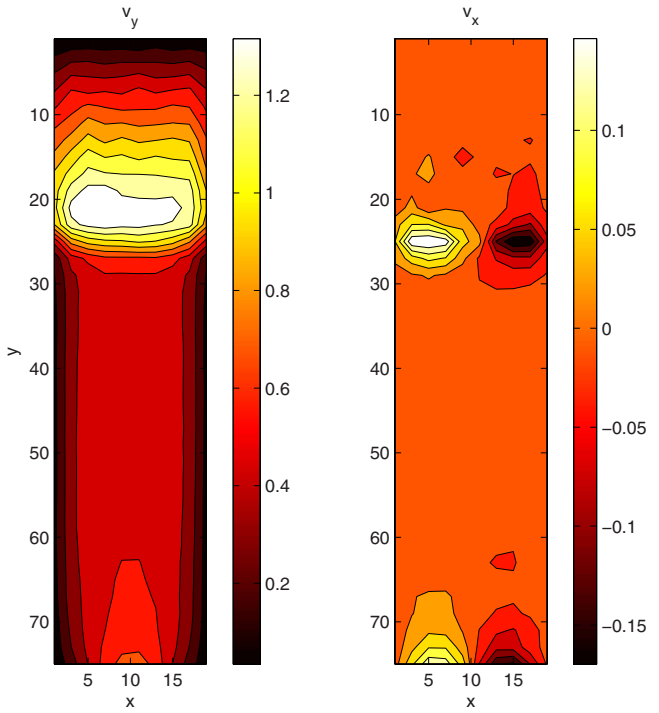

FIG. 1. (Color online) Contour plot of the time-averaged spatial profile of the velocity components. (a) shows the component parallel to the flow, and (b) shows the component of velocity perpendicular to the flow. We focus on the region where the velocity remains approximately constant.

$$\boldsymbol{v}(\boldsymbol{r},t) = \sum_j \boldsymbol{u}_j(t)/N_j, \tag{2}$$

where $\boldsymbol{u}_j$ are the velocities of the N_j particles whose centers lie inside a box of center coordinates $\boldsymbol{r}=(x,y)$ at a given instant t. We do this separately for the vertical (v_y, parallel to flow) and horizontal (v_x, perpendicular to the flow direction) velocity components.

Figure 1 shows the time-averaged profile of the velocity components for the slowest flow rate we report, $v_{\text{flow}}=0.60$, in units of particle diameters per simulation time. Figure 1(a) shows the vertical velocity component v_y over the entire hopper. There is an acceleration region near the top of the hopper—particles are introduced here and accelerate under gravity before they reach an asymptotic density and velocity. For all the analysis described in the rest of the paper, we will focus on this region of constant velocity, extending from $y=35$ to $y=70$. The correlation functions we will present will also exclude the shear layer near the wall, where the velocity is smaller, but nonzero. Figure 1(b) shows the horizontal velocity component field v_x, which is structureless in the region of constant vertical velocity. In the acceleration region, the particles on either side seem to be moving towards the center.

We now look at the variation of the flow profiles for the vertical velocity as the flow rate changes. This is shown in Fig. 2 and is similar to the profile seen in experiments on granular flow [9]. The unscaled flow profiles are shown in the inset for the different flow velocities, and these curves

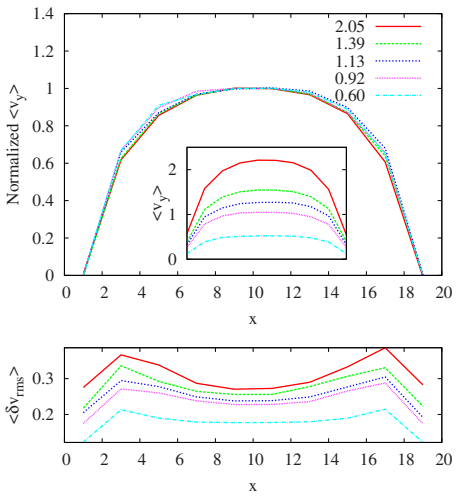

FIG. 2. (Color online) (a) The normalized profiles of the average velocity as a function of x for fixed $y=50$ for five different flow velocities all collapse onto a single curve. The inset shows the unnormalized profiles for the same set of flow rates. (b) The profiles of the rms fluctuations in the velocity for the same flow rates.

show that the mean velocity at the center decreases as the opening at the base of the hopper narrows. We find that these profiles can be collapsed onto the same curve when they are scaled as follows: $(\langle v\rangle-\langle v_s\rangle)/(\langle v_c\rangle-\langle v_s\rangle)$, where v_c is the velocity at the center and v_s the velocity on the sides of the tube. The scaling demonstrates that there is a flow-independent profile which is nonparabolic. This behavior has also been seen in experiments on colloidal flow in a capillary [27]: the question of the origin of this behavior remains an open one.

The time-averaged stress fields are calculated by a similar coarse-graining procedure. The box collisional stress is defined as follows:

$$\sigma^{\mu\nu}(\boldsymbol{r},t) = \frac{1}{\tau A}\sum_{\text{collisions in }\tau} I^{\mu} r^{\nu}, \tag{3}$$

where we sum over all collisions in a box occurring within the time interval $[t,t+\tau]$. $\boldsymbol{I}$ is the impulse transferred at the moment of collision, $\boldsymbol{r}$ the center-to-center vector between colliding particles, and A the box area. Since the particles are hard disks with no interparticle friction, all the momentum transfer is in the direction of the vector separating the centers of the two colliding particles. The above expression then gives us the four stress components in the laboratory frame. We pick an averaging time interval τ that is long compared to the typical collision time but short compared to the time taken for a particle to fall through its own diameter. These scales are well separated in a dense flow: both in experiments and in our simulation a particle undergoes many collisions in the time it takes to fall through its own diameter. Thus while the velocity profiles indicate that the central region of the hopper is moving as a plug, the flow is highly collisional and far from static, as found earlier in experiments [29] and subsequently in simulations [17].

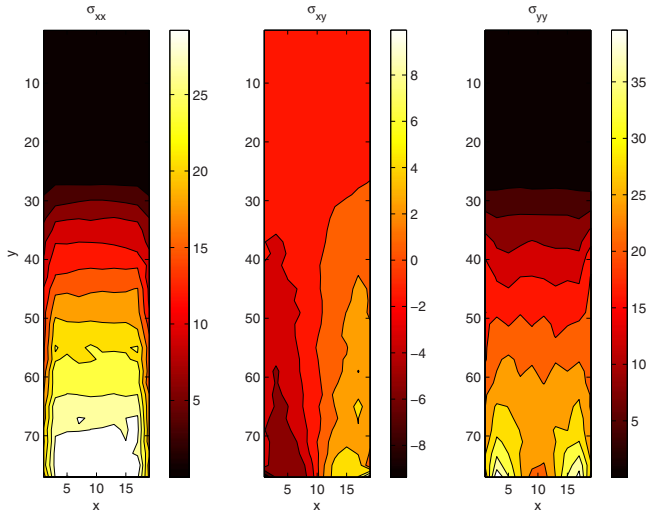

FIG. 3. (Color online) Contour plots of the time-averaged profiles of the stress tensor components (a) σ_{xx} (horizontal pressure), (b) σ_{xy} (shear stress), and (c) σ_{yy} (vertical pressure).

The time-averaged profiles of the stress components are shown in Fig. 3. These are calculated as indicated in the previous paragraph and averaged over the duration of the entire simulation. Figures 3(a) and 3(c) show the normal stress components in the x and y directions, respectively. Note the similarity in structure in both, with a positive gradient in both σ_{xx} and σ_{yy} in the direction of flow. Thus there is an overall gradient in the pressure in the region of constant average velocity. Since we only include the collisional contributions to the stress, there is zero pressure in the acceleration region at the top of the tube since there are no collisions occurring in this region. Figure 3(b) shows the shear-stress component. The shear stress changes sign from the left-hand side to the right-hand side of the tube and has a gradient in the horizontal direction. This appears consistent with the formation of archlike structures that span the tube, arising from chains of frequently colliding particles that were reported earlier [18]. Momentum transfer occurs along the collisional chain and into the walls, but the direction of the wall normal changes from one side of the tube to the other. The stress tensor is symmetric on average $\sigma_{xy}=\sigma_{yx}$ since there is no net torque on the system.

The profile of the time-averaged first normal stress difference $\langle\sigma_N\rangle=\langle\sigma_{yy}-\sigma_{xx}\rangle$ as a function of x is shown in Fig. 4 for all the flow rates studied, and the profile of the time-averaged shear stress $\langle\sigma_{xy}\rangle$ is shown in Fig. 5. These have been averaged over the vertical region ranging from $y=45$ to $y=55$. Figure 5 shows that the shear stress changes sign from one end of the tube to the other for all flow rates, consistent with the presence of collision chains as mentioned earlier in the context of Fig. 3; furthermore, we see that the slope of $\langle\sigma_{xy}\rangle$ as a function of x changes with flow rate—we will discuss this further in the next paragraph. Note that $\langle\sigma_N\rangle$ is close to zero near the center, but large near the boundaries. This non-Newtonian behavior of $\langle\sigma_N\rangle$ is not dictated by any conservation law, but appears to arise due to friction at the walls. Under shear, dense granular flows can have negative normal stress [28], but we find the normal stress stays large

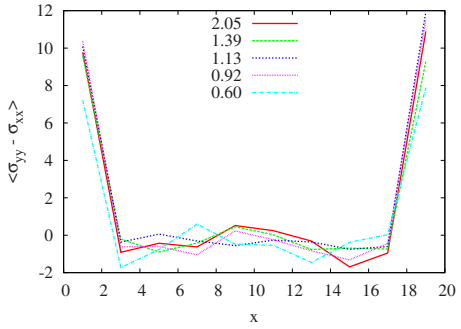

FIG. 4. (Color online) Time-averaged profile of the first normal stress difference $\langle\sigma_N\rangle=\langle\sigma_{yy}-\sigma_{xx}\rangle$ as a function of the horizontal variable x for five different flow rates.

and positive near the boundaries, and approaches zero at the center. A continuum description of the flow would need to take into account this structure of the normal stress, as well as explain the nonparabolic flow profile of the vertical velocity, Fig. 2.

Momentum conservation dictates that

$$\partial_t \rho v_i + \partial_j \rho v_i v_j = \partial_j \sigma_{ij} + f_i, \tag{4}$$

where ρ is the local density, v_i the velocity, σ_{ij} the stress tensor, and f_i the external force. Under steady-state conditions, both terms on the left-hand side are zero and the stress tensor on the right-hand side is purely collisional. In particular,

$$\partial_x \sigma_{xy} + \partial_y \sigma_{yy} + f_y = 0; \tag{5}$$

i.e., the sum of the vertical gradient in the vertical pressure and the horizontal gradient in the shear stress supports the weight of the column. For our range of parameters, we find that the relative importance of these two terms changes smoothly with the flow rate: at high flow rates, the horizontal gradient of the shear stress dominates, but at low flow rates, the vertical gradient in the vertical pressure component is larger, as shown in Fig. 6. Denniston and Li [17] reported that the horizontal gradient in the shear stress gave a much larger contribution, but this was for a single flow rate, which was larger than the largest flow rate we study and is therefore consistent with our findings.

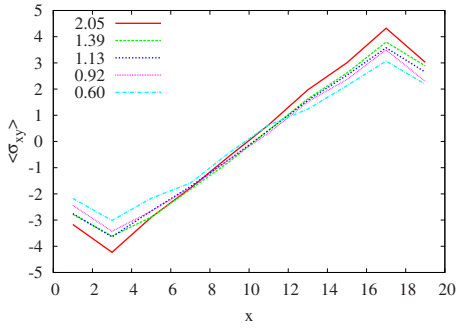

FIG. 5. (Color online) Time-averaged profile of the shear stress $\langle\sigma_{xy}\rangle$ as a function of the horizontal variable x for five different flow rates.

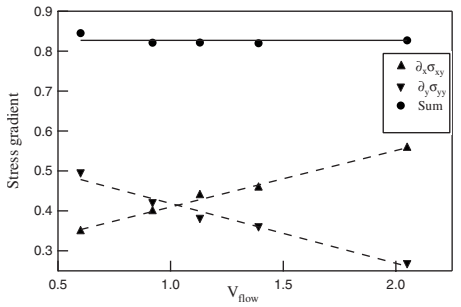

FIG. 6. A comparison of the spatial derivatives of the stress components $\partial_x\sigma_{xy}$ (averaged over y values in the region of constant vertical velocity) and $\partial_y\sigma_{yy}$ (averaged over x values, excluding the boundaries) that support the weight of the column. Note that their sum stays approximately constant as the flow rate changes, but at high flow velocities the horizontal gradient of the shear stress dominates, whereas the vertical gradient of the vertical pressure becomes more important as the flow rate decreases.

B. Relaxation time: Velocity and stress autocorrelations

We first examine fluctuations in the kinematic variables and how closely fluctuations at a given spatial point in the flow remain correlated in time. The normalized autocorrelation $C_i(r,t)$ of the velocity component $v_i(r,t)$ at a spatial point r is defined as

$$C_i(r,t) = \frac{\langle \Delta v_i(r,t+\tau)\Delta v_i(r,t)\rangle}{\langle [\Delta v_i(r,t)]^2\rangle}, \tag{6}$$

where $\Delta v_i(r,t)=v_i(r,t)-\langle v_i\rangle$ represents the time-dependent fluctuation of the velocity component, $i=x$ or y, and the averages are over time. This quantity is then spatially averaged over all the boxes in the region of constant velocity, giving

$$\langle v_i(t)v_i(0)\rangle = \frac{1}{N_s}\sum_r C_i(r,t), \tag{7}$$

where N_s is the number of boxes summed over.

The autocorrelations of the fluctuations in both velocity components are shown as a function of time in Figs. 7 and 8 for five different flow velocities. The correlations fall off fairly rapidly at short times at all flow rates. As one moves from fast to slow flow (from left to right in the figures), there

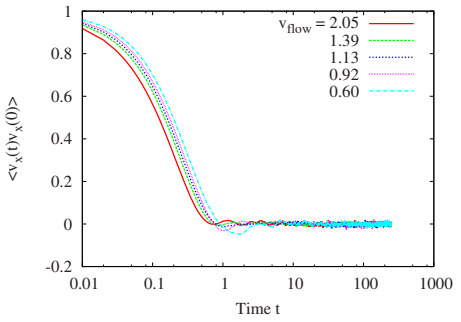

FIG. 7. (Color online) Autocorrelation of the velocity component perpendicular to the flow at at five different flow rates. The flow rates are expressed in units of particle diameters per simulation time.

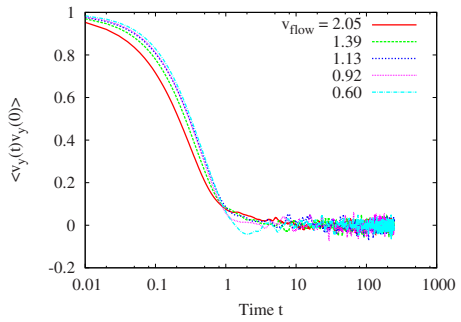

FIG. 8. (Color online) Autocorrelation of the velocity component parallel to the flow at the same five flow rates.

is a consistent but slow trend towards increasing relaxation time as the flow rate decreases (note that the x-axis scale has been made logarithmic in the figure to emphasize this). Thus temporal correlations in the velocity fluctuations do not provide a strong indication of an impending jam as the flow rate decreases.

Clearer evidence of a growth in the relaxation time scale is seen in the stress. The autocorrelation of the fluctuations in the stress components $\langle \sigma_{ij}(t)\sigma_{ij}(0)\rangle$ is defined exactly the same way as for the velocity components, as indicated in Eqs. (6) and (7). These autocorrelations decay with time with some characteristic time scale, and evidence for an increase in the decay time scale as the flow rate decreases is seen in all three components. However, the increase in time scale is most pronounced for the shear stress σ_{xy}, and the autocorrelation of this stress component is shown in Fig. 9 for five flow rates. Note that the time axis in this figure is logarithmic, and after an initial drop at very short times (equivalent to one averaging time step), the decay of the stress autocorrelations is logarithmic at intermediate times. The change with flow rate of the autocorrelation time (measured as described in the next paragraph) of the two other stress components, the horizontal and vertical pressures σ_{xx} and σ_{yy}, respectively, is similar to that seen for the two velocity components in Figs. 7 and 8.

We extract a time scale from these autocorrelation functions by measuring the time at which the (normalized) autocorrelation function drops to 0.1. This time τ is plotted as a function of inverse mean flow velocity in Fig. 10. Note that while the autocorrelation time associated with the two velocity components and the two diagonal components of stress

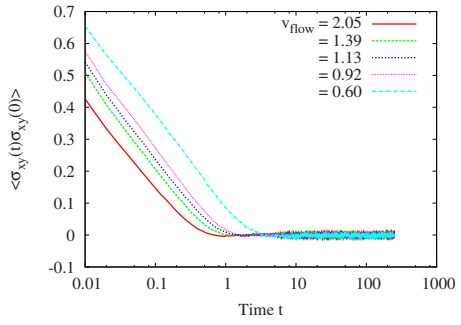

FIG. 9. (Color online) Autocorrelation of the shear stress at the same five flow rates.

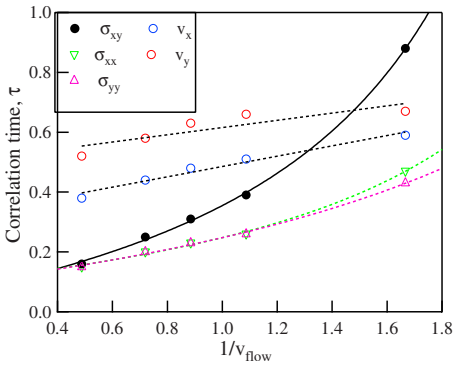

FIG. 10. (Color online) Time at which the autocorrelations of the different velocity and stress components drop to 0.1 as a function of the inverse flow velocity. The lines are intended as guides to the eye and are obtained from quadratic fits to the data. Note the time scale associated with the shear stress shows a much greater dependence on flow velocity.

all increase as flow rate decreases, the time scale associated with the shear stress increases more rapidly than the others as the flow slows. This increase is also more rapid than linear (the lines in the figure, intended as guides to the eye, are fits to quadratics). As we shall see in the next section, this increase in autocorrelation time leads to the growth of a region that flows like a plug and is consistent with the presence of chains of frequently colliding particles that begin to span the system at the lower flow rates. Evidence that the dominant contribution to the principal axis of the collisional stress tensor comes from the most frequently colliding particles was presented in earlier work [19] on the same simulations. There we found that the timescale associated with the fluctuations of the principal axis of the stress increased linearly with inverse flow rate.

C. Length scales: Spatial correlations in velocity and stress

We next examine the spatial correlations in the fluctuations of both kinematic and dynamic variables. We define the normalized equal-time spatial correlation function of the velocity fluctuations as a function of separation as follows:

$$\langle v_i(\boldsymbol{r})v_i(0)\rangle = \frac{\Sigma_{\boldsymbol{r}_i}\Sigma_i \Delta v_i(\boldsymbol{r}_i,t)\Delta v_i(\boldsymbol{r}_i+\Delta\boldsymbol{r},t)}{N_s\Sigma_i[\Delta v_i(\boldsymbol{r}_i,t)]^2}, \qquad (8)$$

where N_s is the number of spatial points (boxes) summed over and $\Delta v_i(r,t)$ represents the velocity fluctuation relative to the long-time average.

The spatial correlations for the vertical velocity component $\langle v_y(y)v_y(0)\rangle$ are shown as a function of vertical separation y in Fig. 11 for five different flow rates. Note that as the flow rate decreases, the spatial correlation dies off more slowly, suggestive of an increasing length scale. Our numerical results are shown by the points in the figure, and the solid lines are fits to stretched exponential behavior—we shall discuss these fits further in what follows. The figure shows that the correlations are very long range and complete decorrelation is not achieved across the entire region of analysis. We are beginning to systematically investigate finite-size effects

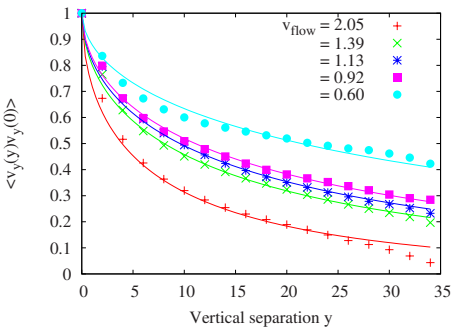

FIG. 11. (Color online) The equal time spatial correlation function of the vertical velocity component is shown as a function of vertical separation at five different flow rates. The points are obtained from the numerical simulation, and the solid lines represent fits to the data using the stretched exponential function $\exp[-(y/\lambda)^{0.55}]$ with λ as the only fitting parameter.

on the growing length and time scales in order to better characterize the nature of the jamming transition.

The spatial correlation function for the horizontal velocity component $v_x(y)$ is shown in Fig. 12, along with the curves from the previous figure using the same color scheme for the same set of flow rates. Figure 12 shows that spatial correlations in the horizontal velocity component die out very rapidly and there is no systematic change in the spatial extent of the correlations with flow rate. The same trend is seen when the spatial correlations of both velocity components are computed as a function of horizontal separation $\langle v_i(x)v_i(0)\rangle$.

We next compute the equal-time spatial correlation function for the components of the stress tensor exactly as in Eq. (8). The spatial correlations for the vertical pressure $\langle \sigma_{yy}(y)\sigma_{yy}(0)\rangle$ are shown as a function of vertical separation y in Fig. 13 for five different flow rates. This looks very similar to the behavior seen in Fig. 11 for the spatial correlations in the vertical velocity. Once again, the points are obtained from the simulations and the lines represent fits to stretched exponential behavior.

Spatial correlations in the horizontal pressure $\langle \sigma_{xx}(x)\sigma_{xx}(0)\rangle$ as a function of horizontal separation show very similar behavior to that seen in Fig. 13, but we have not

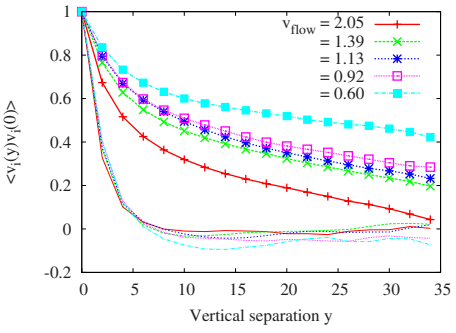

FIG. 12. (Color online) Comparison of the equal time spatial correlation function of the vertical velocity component from the previous graph (lines and symbols) to the spatial correlations of the horizontal velocity component (lines) as a function of vertical separation at the same five flow rates. No fits are shown in this plot, and the lines simply connect the points.

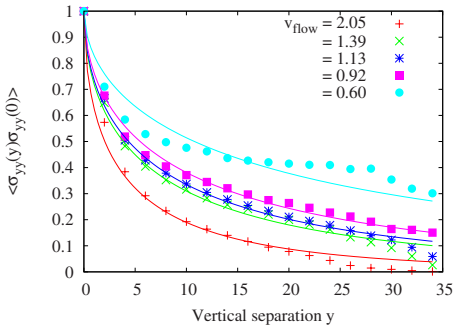

FIG. 13. (Color online) Plots of the equal time spatial correlation functions of the vertical pressure fluctuations $\Delta\sigma_{yy}$ as a function of vertical separation at five flow rates. The points represent the numerical data, and the solid lines are once again fits to stretched exponential behavior $\exp[-(y/\lambda)^{0.55}]$.

shown it because of the limited range available in the x direction. Equal-time spatial correlations of the vertical pressure σ_{yy} as a function of horizontal separation x and those of the horizontal pressure σ_{xx} as a function of vertical separation y (both not shown) also have the same trend as a function of flow rate, but show a less pronounced change than the correlations seen in Fig. 13. The vertical velocity also shows no significant spatial correlations in the horizontal direction. Interestingly, the shear stress shows no spatial correlations: the equal-time spatial correlation function in σ_{xy} dies very rapidly and shows no change as a function of flow rate. We will return to this observation in the next section.

We can extract from Figs. 11 and 13 a characteristic length scale λ by fitting both spatial correlation functions to a stretched exponential decay function, $\exp[-(y/\lambda)^{0.55}]$, where λ is the only fitting parameter. (We estimated the exponent 0.55 by first doing a two-parameter fit of the curves.) The fits are represented by solid lines in the two figures. We plot λ as a function of inverse flow rate in Fig. 14. Though the λ values obtained from v_y and σ_{yy} are not the same, both increase faster than linearly with inverse flow rate and follow the same trend.

It is clear from Figs. 11 and 13 that the correlation functions are not perfectly described by stretched exponential behavior: the fits work best at intermediate flow velocities, but there are deviations at slow and fast flow, and the agreement

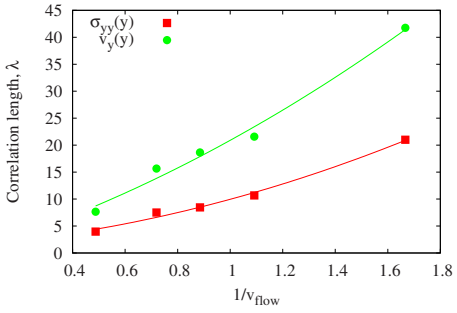

FIG. 14. (Color online) The length scales λ obtained from fitting the equal-time spatial correlation functions $\langle v_y(y)v_y(0)\rangle$ and $\langle\sigma_{yy}(y)\sigma_{yy}(0)\rangle$ to a stretched exponential decay $\exp[-(y/\lambda)^{0.55}]$ are plotted as a function of inverse flow rate.

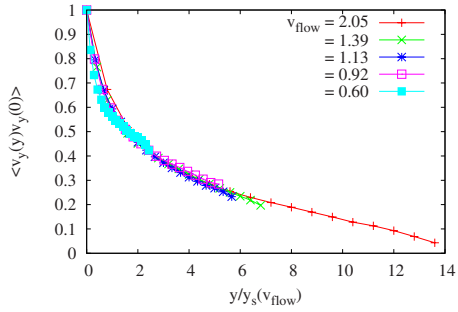

FIG. 15. (Color online) The equal time spatial correlation function of the vertical velocity component $\langle v_y(y)v_y(0)\rangle$ is plotted as a function of scaled vertical position $y/y_s(v_{flow})$, where $y_s(v_{flow})$ is a flow-velocity-dependent length. The curves do not superimpose exactly, with a significant change in shape as the flow approaches jamming.

is very poor at the slowest flow rate. We tried other ways of extracting a length: by measuring the distance at which the correlation function drops to a fixed fraction—say, 0.4—and by scaling the horizontal axis by a flow-velocity-dependent length to superimpose all the curves. In all these cases, though the actual λ values change, the dependence of the length on flow velocity shows the same trend as in Fig. 14. Rescaling the horizontal axis also shows us that the shape of the correlation function changes as one approaches jamming; see Fig. 15.

Finally, the length scales λ extracted from the vertical velocity v_y and pressure σ_{yy} fluctuations (Fig. 14) as well as the time scale τ obtained from the autocorrelations of the shear stress σ_{xy} (Fig. 10) are plotted as a function of $A-A_0$ in Fig. 16. Here A is the size of the opening at the bottom of the hopper and $A_0=2.2$ is the size at which the flow velocity extrapolates to zero. (The flow velocity decreases roughly linearly with the size of the opening.) All three quantities appear to display power-law behavior as indicated by the solid line fits, though our dynamic range is too small to say this more definitively. The power law exponents for the length scale in the vertical velocity fluctuations is -1.3, close to the -1.4 exponent seen for the length scale coming from

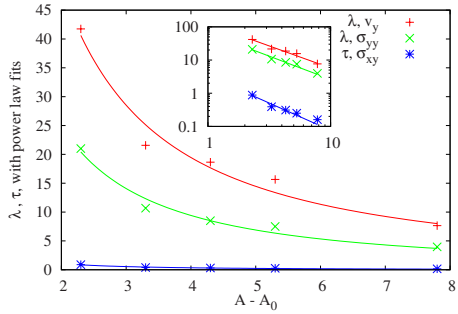

FIG. 16. (Color online) The length scales λ obtained from the equal-time spatial correlation functions of v_y and σ_{yy} and the time scale τ from the autocorrelation of σ_{xy} are plotted as a function $A-A_0$, where A is the size of the opening and A_0 the opening at which the flow velocity extrapolates to zero. The solid lines are power-law fits with exponents -1.3 (λ, v_y), -1.4 (λ, σ_{yy}), and -1.6 (τ, σ_{xy}). The inset shows the same set of data and fits on a log-log plot.

the vertical pressure fluctuations. The exponent for the time-scale in the shear stress fluctuations is −1.6. It is difficult to make measurements over a larger range of flow velocities for this particular system, since a steady state is hard to achieve when the opening is too wide and the flow tends to jam intermittently when the opening is less than four particle diameters. We plan to run the simulation for larger systems which would help us better measure these power laws.

IV. DISCUSSION

We have observed a growing length scale in dense gravity-driven granular flow as the flow rate decreases towards jamming. This length scale characterizes the decay of the two-point spatial correlation functions of the velocity and the normal stress. Correspondingly, there is a growth in the relaxation time associated with the shear stress. By contrast, the relaxation times of the velocity fluctuations grow very little, and no accompanying structural changes in the density are seen. Thus increasing temporal correlations in the shear-stress fluctuations are closely tracked by spatial correlations in the flow velocity and the pressure. Both the relaxation times and length scales derived from these two-point correlation functions appear to increase as power laws of the opening size in the dynamic range available to us.

Our observation of an increasing length scale is consistent with the diverging length scale seen in recent simulations of soft frictionless disks under shear [5]. While the latter system is different in the details and is dominated by slow relaxation of stress in contrast to the highly collisional regime we study, the agreement between the two suggests that jamming is a true cooperative phenomenon, reminiscent of a second-order phase transition, with, however, an interesting difference. In standard critical phenomena it is usually a diverging length scale that signals the development of order in the system and leads to a divergence in the relaxation times. Here, by contrast, our observations indicate that it is the time scale associated with the collisional dynamics that leads to an increase in length scale in the stress. A connection between the structure of the stress tensor and frequently colliding chains of particles was previously established [19]. The increase in autocorrelation time of the shear stress as the flow rate decreases indicates an increase in lifetime of these collision chains. These chains form and break up repeatedly during the flow, and while they lead to an increased autocorrelation time in the *shear stress*, no corresponding increase in the spatial correlation of the shear-stress fluctuations is seen. The effect of their formation is instead to make the system flow as a plug, which is seen in increased spatial correlations of the *normal* stresses and vertical velocity. The increase in the equal-time spatial correlations of the velocity can be construed as a further sign that collisions in the system are becoming less random. The time between collisions decreases along with the flow rate, so there are many more collisions in a given time interval. Thus collisions must occur in a spatially correlated way.

An interesting scenario, which we are in the process of investigating, is whether an increasing length scale in two-point spatial correlation functions of the velocity, as seen here, can lead to the type of behavior observed in four-point density correlation functions [24,30].

The scaling of the time-averaged flow profiles of the velocity indicates that the size of the shear zone does not change with flow rate. We also find a large positive first normal stress difference near the walls, which points to the importance of friction at the walls. This friction slows down the flow and leads to the formation of frequently colliding chains of particles, which in turn leads to strong spatial correlations in the flow. Any effective continuum theory of granular flow must explain the shape of these profiles. An essential ingredient of a continuum model would be the strong spatial correlations in the velocity. The Boltzmann assumption of uncorrelated velocities breaks down here, and one approach to developing a continuum model would be to begin with an assumption of spatially correlated velocities.

Our results agree well with experiments on gravity-driven hopper flow in two dimensions [11] in which force-velocity correlations have long-range effects. Our simulations make it clear that these correlations are also present in the spatial structure of the stress fluctuations. Our observation that an increasing length is associated with the normal components of the stress and not in the shear component poses a further puzzle.

ACKNOWLEDGMENTS

We wish to acknowledge useful discussions with Narayanan Menon, Nalini Easwar, Giulio Biroli, Andrea Liu, and Douglas Durian. We thank Melanie Finn and Anna-Lisa Baksmaty, for their contributions to this project. S.T. and B.C. thank the Aspen Center for Physics for their hospitality. B.C. acknowledges the support of Grant No. NSF-DMR 0549762.

[1] H. M. Jaeger, S. R. Nagel, and R. P. Behringer, Rev. Mod. Phys. **68**, 1259 (1996).
[2] A. J. Liu and S. R. Nagel, Nature (London) **396**, 21 (1998).
[3] L. E. Silbert, A. J. Liu, and S. R. Nagel, Phys. Rev. Lett. **95**, 098301 (2005).
[4] M. Wyart, S. R. Nagel, and T. A. Witten, Europhys. Lett. **72**, 486 (2005).
[5] P. Olsson and S. Teitel, Phys. Rev. Lett. **99**, 178001 (2007).
[6] P. Dantu, Ann. Ponts Chaussees **4**, 144 (1967).
[7] C. H. Liu *et al.*, Science **269**, 513 (1995).
[8] J. Choi, A. Kudrolli, R. R. Rosales, and M. Z. Bazant, Phys. Rev. Lett. **92**, 174301 (2004).
[9] S. Moka and P. R. Nott, Phys. Rev. Lett. **95**, 068003 (2005).
[10] E. Longhi, N. Easwar, and N. Menon, Phys. Rev. Lett. **89**, 045501 (2002).
[11] Emily Gardel, E. Keene, S. Dragulin, N. Easwar, and N. Menon, e-print arXiv:cond-mat/0601022.
[12] D. Howell, R. P. Behringer, and C. Veje, Phys. Rev. Lett. **82**,

5241 (1999).
[13] T. S. Majmudar and R. S. Behringer, Nature (London) **435**, 1079 (2005).
[14] E. I. Corwin, H. M. Jaeger, and S. R. Nagel, Nature (London) **435**, 1075 (2005).
[15] D. Bonamy, F. Daviaud, L. Laurent, M. Bonetti, and J. P. Bouchaud, Phys. Rev. Lett. **89**, 034301 (2002).
[16] O. Pouliquen, Phys. Rev. Lett. **93**, 248001 (2004).
[17] C. Denniston and H. Li, Phys. Rev. E **59**, 3289 (1999).
[18] A. Ferguson, B. Fisher, and B. Chakraborty, Europhys. Lett. **66**, 277 (2004).
[19] A. Ferguson and B. Chakraborty, Phys. Rev. E **73**, 011303 (2006).
[20] M. A. Ediger, Annu. Rev. Phys. Chem. **51**, 99 (2000).
[21] C. Dasgupta, A. V. Indrani, S. Ramaswamy, and M. K. Phani, Europhys. Lett. **15**, 307 (1991).
[22] S. C. Glotzer, V. N. Novikov, and T. B. Schroder, J. Chem. Phys. **112**, 509 (2000).
[23] E. R. Weeks, J. C. Crocker, A. C. Levitt, A. Schofield, and D. A. Weitz, Science **287**, 627 (2000).
[24] O. Dauchot, G. Marty, and G. Biroli, Phys. Rev. Lett. **95**, 265701 (2005).
[25] M. M. Hurley and P. Harrowell, Phys. Rev. E **52**, 1694 (1995).
[26] A. Ferguson and B. Chakraborty, Europhys. Lett. **78**, 28003 (2007).
[27] L. Isa, R. Besseling, and W. C. K. Poon, Phys. Rev. Lett. **98**, 198305 (2007).
[28] M. Alam and S. Luding, J. Fluid Mech. **476**, 69 (2003).
[29] N. Menon and D. J. Durian, Science **275**, 1920 (1997).
[30] A. S. Keys, A. R. Abate, S. C. Glotzer, and D. J. Durian, Nat. Phys. **3**, 260 (2007).